Fuentes López, C.; Ruiz Rico, M.; Fuentes López, A.; Ruiz, MJ.; Barat Baviera, JM. (2020). Degradation of silica particles functionalised with essential oil components under simulated physiological conditions. Journal of Hazardous Materials. 339:1-10. https://doi.org/10.1016/j.jhazmat.2020.123120

Degradation of silica particles functionalised with essential oil components under simulated physiological conditions

Cristina Fuentes[a], María Ruiz-Rico[a], Ana Fuentes[a], María José Ruiz[b], José Manuel Barat[a]

[a]Department of Food Technology, Universitat Politècnica de València. Camino de Vera s/n, 46022, Valencia, Spain: crifuelp@upvnet.upv.es

[b]Laboratory of Toxicology, Faculty of Pharmacy, Universitat de València, Av. Vicent Andrés Estellés s/n, 46100 Burjassot, Valencia, Spain

Keywords: Silica; MCM-41; Functionalisation; *In vitro* digestion; Artificial lysosomal fluid

Abstract

In this work, the biodurability of three silica particle types (synthetic amourphous silica, MCM-41 microparticles, MCM-41 nanoparticles) functionalised with three different essential oil components (carvacrol, eugenol, vanillin) was studied under conditions that represented the human gastrointestinal tract and lysosomal fluid. The effect of particle type, surface immobilised component and mass quantity on the physico-chemical properties of particles and silicon dissolution was determined. Exposure to biological fluids did not bring about changes in the zeta potential values or particle size distribution of the bare or functionalised materials, but the *in vitro* digestion process partially degraded the structure of the MCM-41 nanoparticles. Functionalisation preserved the structure of the MCM-41 nanoparticles after simulating an *in vitro* digestion process, and significantly decreased the amount of silicon dissolved after exposing different particles to both physiological conditions, independently of the essential oil component anchored to their surface. The MCM-41 microparticles showed the highest solubility, while synthetic amorphous silica presented the lowest levels of dissolved silicon. The study of these modified silica particles under physiological conditions could help to predict the toxicological behaviour of these new materials.

1. **Introduction**

Particle biodurability is defined as its ability to resist enzymatic biodegradation or chemical disintegration through dissolution, and is considered an important property that should be investigated to evaluate particles' toxicity (Utembe et al., 2015). Biodurability can be studied by the dissolution of materials in acellular physiological fluids that mimic intracellular or extracellular conditions. Of these, the degradation rate under conditions that represented the human gastrointestinal tract and lysosomal fluid is considered key information in the structured approach to identify and characterise toxicological hazards after oral exposure (Hardy et al., 2018). A simulated *in vitro* digestion process (SID) can be used to investigate the stability of particles under conditions that mimic the gastrointestinal tract. Once in the body, if the material does not quickly degrade, it may not be easily eliminated and can accumulate over time. The lysosome is the commonest intracellular compartment for particles sequestration and degradation. For this reason, artificial lysosomal fluid (ALF) that simulates the inorganic acidic environment within lysosomes has been widely used to study the durability of different materials after phagocytosis into cells (Cho et al. 2012; Henderson et al. 2014; Stebounova, Guio, and Grassian 2011).

Synthetic amorphous silica (SAS) has been used in a variety of oral applications, including foodstuffs (Pennington, 1991; Villota and Hawkes, 1986), pharmaceuticals (Colas and Rafidison, 2005) or dentistry materials (Lührs and Geurtsen, 2009). The presence of silanol groups (Si-OH) on the inner and outer surfaces of silica materials facilitates its chemical functionalisation by specific groups to increase their applicability (Diab et al., 2017). In the last few decades, mobile crystalline material 41 (MCM-41), an amorphous porous silica material, has been proposed for a wide range of new biotechnological applications (Flynn et al., 2019; Manzano et al., 2008; Pérez-Esteve et al., 2016b; Wang et al., 2009) due to its unique properties, such as ordered structure, large surface area and big pore volume (ALOthman, 2012). The dissolution behaviour of different types of SAS under biological-like conditions has been demonstrated to differ depending on the nature of the bulk material (He et al., 2011; Roelofs and Vogelsberger, 2004). Moreover, physico-chemical properties like size, morphology, surface area, pore size and surface modification influence the degradability of silica particles (Croissant et al., 2018). These changes may lead to altered toxicological effects compared to the corresponding bare materials (Lin et al., 2011), which indicates the need to develop a case-by-case study of the behaviour of modified materials under physiological conditions and their specific risk assessment.

The aim of the present work was to study the stability of different silica particles under simulated physiological conditions after oral exposure. In particular, we investigated the

degradation behaviour of three types of silica particles (SAS, MCM-41 microparticles, MCM-41 nanoparticles) functionalised with three different essential oil components (EOCs: carvacrol, eugenol, vanillin) which were designed to be used as antimicrobial devices against food-borne pathogens and spoilage microorganisms (Ribes et al., 2019, 2017; Ruiz-Rico et al., 2017). For this purpose, the physico-chemical properties of the materials and the concentration of the dissolved silicon after an *in vitro* digestion process and under conditions representing lysosomal fluid, were determined.

2. Materials and Methods

2.1. Chemicals

Triethanolamine ($TEAH_3$), sodium hydroxide (NaOH), tetraethylorthosilicate (TEOS), *N*-cetyltrimethylammonium bromide (CTAB), paraformaldehyde, (3-aminopropyl) triethoxysilane (APTES), carvacrol (98% w/w), eugenol (99% w/w), hydrochloridric acid (HCl), pepsin, bile extract and pancreatine (all three of porcine origin), and all the other reagents used to prepare SID solutions and ALF, were supplied by Sigma-Aldrich (Madrid, Spain). Vanillin was acquired from Ventós (Barcelona, Spain). Amorphous silica microparticles (SYLYSIA® SY350/FCP; 4 (0.1) μm) were purchased from Silysiamont (Milano, Italy). All the employed materials were of standard analytical grade.

2.2. Mesoporous silica particles synthesis

Mesoporous MCM-41 microparticles. The synthesis of the MCM-41 microparticles was carried out via the 'atrane route' using a molar ratio of reagents: 7 $TEAH_3$: 2 TEOS: 0.52 CTAB: 0.5 NaOH: 180 H_2O. To perform this reaction, a solution of NaOH and $TEAH_3$ was heated to 120ºC and stirred at 300 rpm. The mixture was cooled to 70ºC. After adding TEOS, temperature was increased to 118ºC. CTAB was added to the solution, temperature was lowered again to 70ºC and then 180 mL of distilled water were added by increasing the stirring speed to 600 rpm. A white precipitate formed and the solution was stirred for 1 h at room temperature. After this time, the suspension was placed in a teflon container at 100ºC and kept for 24 h to then be vacuum-filtered and the solid was washed with distilled water to a neutral pH. The obtained material was dried at 72ºC for 24 h and calcined at 550ºC in an oxidant atmosphere for 5 h to remove the organic template (MCM-41 micro).

Synthesis of mesoporous MCM-41 nanoparticles. For the synthesis of the MCM-41 nanoparticles, CTAB (2.74 mM) was dissolved in distilled water at 500 rpm and the NaOH solution (7 mM) was added. The mixture was kept at 80ºC and stirring increased to 1,200 rpm. Then 22.39 mM of TEOS were added drop-wise and a white suspension formed. The reaction

was left stirring at 80ºC for 30 min. After this time, heat was turned off and the reaction was neutralised with 4 mL of the HCl 1M solution (pH~7). Finally, the solid product was centrifuged at 9,500 rpm for 20 min, washed with deionised water and dried at 70ºC. After drying, and like the MCM-41 microparticles, the resulting nanoparticles were calcined (MCM-41 nano).

2.3. Immobilisation of EOCs on the surface of particles and quantification

The functionalisation process of the silica particles with EOCs was done by a three-stage reaction (Fig. 1). First of all, the synthesis of aldehyde derivatives of carvacrol by direct formylation using paraformaldehyde and eugenol was performed according to the Reimer-Tiemann reaction. The presence of an aldehyde group in the vanillin structure allowed this stage to be avoided. In a second stage, the EOC-alkoxysilane derivatives were synthesised by the reaction of APTES with the aldehyde forms of carvacrol and eugenol or pure vanillin. Finally, the alkoxysilane derivatives were covalently anchored to the silanol groups present on the surface of the three different studied silica particles. The functionalisation process is fully described by García-Ríos et al.(2018).

The content of the EOCs grafted on the silica particle's surface was determined by the thermogravimetric analysis (TGA) and the elemental analysis. A TGA/SDTA 851e Mettler Toledo scale (Mettler Toledo Inc., Schwarzenbach, Switzerland) was used for the TGA analysis done with the samples in an oxidising atmosphere (air, 80 mL/min) with a heating programme (heating ramp of 10ºC/min from 25ºC to 1,000ºC) and a heating stage. The elemental analysis for C, H and N was performed by a combustion analysis run in a CHNOS Vario EL III model (Elemental Analyses System GMHB, Langenselbold, Germany).

2.4. In vitro degradation tests

The stability of the different silica particles under two physiological conditions was investigated as an important factor that would influence the toxicity of these materials. Firstly, a stability study under the simulated gastrointestinal tract conditions was conducted to evaluate the degradation of particles after oral ingestion. Secondly, a degradation test under the simulated lysosomal conditions was performed to study the durability of particles after phagocytosis in cells. Dissolution studies were conducted with 11 different particle types: SAS microparticles without mesoporous structure, MCM-41 micro and MCM-41 nano, bare or functionalised with all three EOCs (carvacrol, eugenol, vanillin). Two different mass of particles were studied for each sample: 50 mg (C1) and 100 mg (C2). Each condition was tested in duplicate. A scheme of the experimental procedure herein followed is shown in Figure 2.

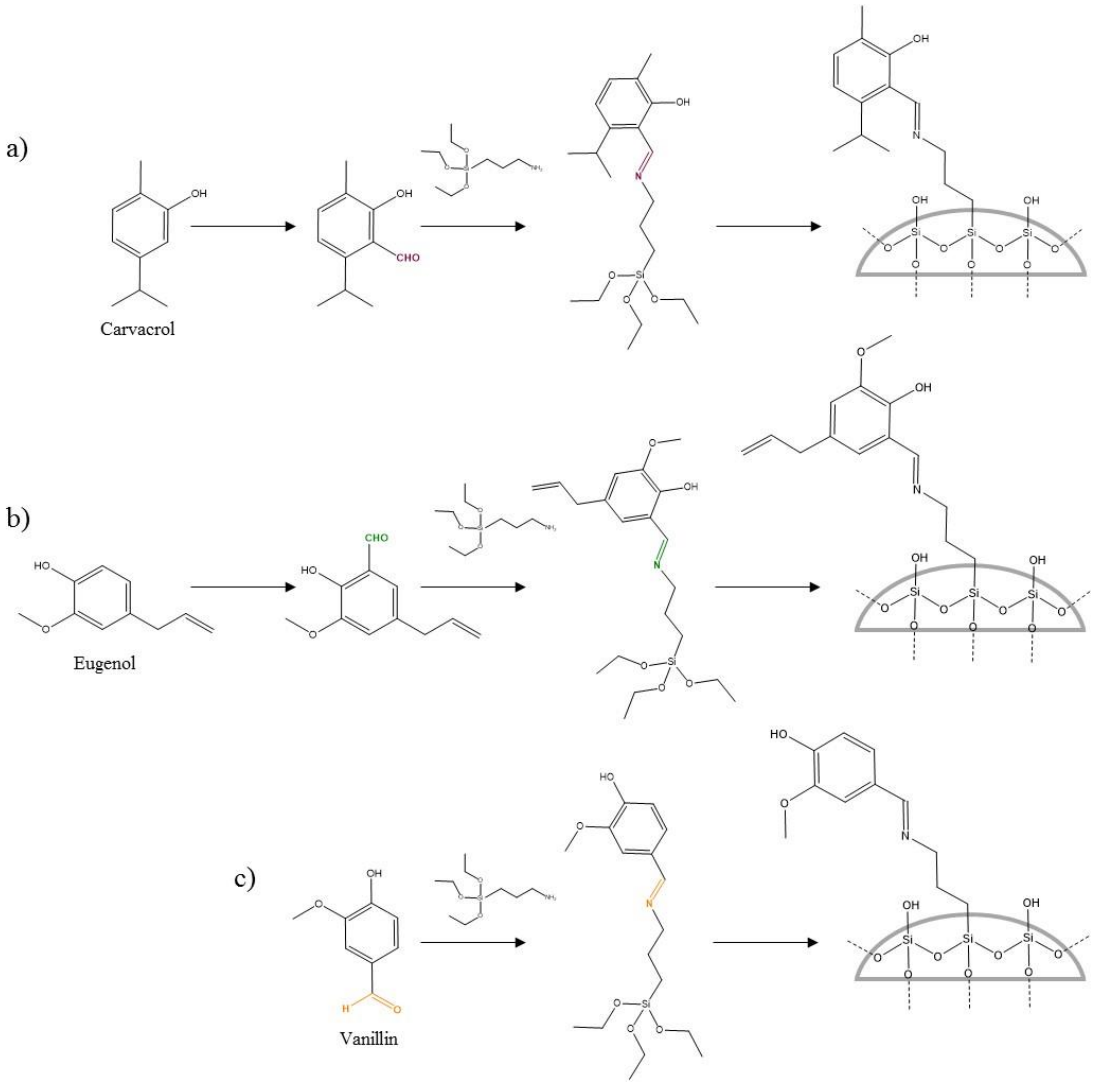

Fig. 1. Synthetic route for the formation of the carvacrol (a), eugenol (b) and vanillin (c) functionalised silica particles. Firstly, aldehyde derivatives of carvacrol and eugenol were synthesised (substitution at the ortho position provided as an example). Secondly the aldehydes of carvacrol and eugenol or pure vanillin were transformed into the corresponding alkoxysilane derivatives by a reaction with APTES. Finally, alkoxysilane derivatives were anchored to the surface of the three studied types of silica particles (SAS, MCM-41 micro, MCM-41 nano).

2.4.1. In vitro gastrointestinal digestion

A static *in vitro* digestion model was used to simulate the digestion of silica particles by the gastrointestinal tract. The *in vitro* digestion model consisted of three steps to simulate the physiological conditions of the human gastrointestinal tract: saliva, gastric, small intestine digestion. The standardised protocol based on an international consensus developed by the

COST INFOGEST network (Brodkorb et al., 2019; Minekus et al., 2014) was employed with minor modifications. Briefly, particles were diluted in 5 mL of simulated salivary fluid (SSF) with 1.5 mM of $CaCl_2$. The mixture was stirred for 2 min and, due to small particle size, mastication was ignored. Subsequently, 5 mL of simulated gastric fluid (SGF) with 0.15 mM of $CaCl_2$ and the pepsin enzyme were added and incubated under agitation at pH 3.0 for 2 h. Finally, 10 mL of simulated intestinal fluid (SIG) with 0.6 mM of $CaCl_2$, bile salts and pancreatic enzymes were added and incubated at pH 7 for another 2-hour period. At the end of the digestion process, samples were adjusted to pH 5 to stop the digestion reaction and were then kept at -40ºC until the analysis. Throughout the procedure, digestion tubes were orbitally stirred (100 rpm) at 37ºC and the pH values of the digestive fluids were readjusted, if necessary, with NaOH (1 M) or HCl (6 M). The SID procedure is summarised in Figure S1. An *in vitro* digestion assay without enzymes and bile extracts was run in parallel to avoid the organic components interfering with the measurements of the particles' physico-chemical properties.

Digestive juices were prepared the day before and heated to 37ºC before the experiment. The constituents and concentrations of the different simulated digestion fluids are fully described by Brodkorb et al. (2019).

2.4.2. Stability in lysosomal fluid

In order to assess the stability of the different silica particles under lysosomal conditions, dissolution in ALF was evaluated. The ALF solution was prepared in advance using the chemical composition and concentrations described by Stopford et al. (2003). The solution was heated to 37ºC. Then 50 mL were added to each sample tube. Samples were continuously stirred at 100 rpm on an orbital shaker for the time that the experiment took. Solutions were monitored to note any pH changes occurring during the experiment. The control blanks, consisting solely of ALF, were sampled and continuously stirred in the same way as the test solutions. Three different time points were investigated: exposures of 24, 48 and 72 h. At each sampling point, samples were centrifuged at 9,500 rpm for 10 min and 5 mL of each supernatant were collected, while an equal volume of fresh ALF solution was added to each tube. At the end of the SID assay and after 72 h of the ALF treatment, particles were recovered by centrifugation (9,500 rpm; 10 min) for their characterisation. Supernatants were stored at -40ºC until the analysis.

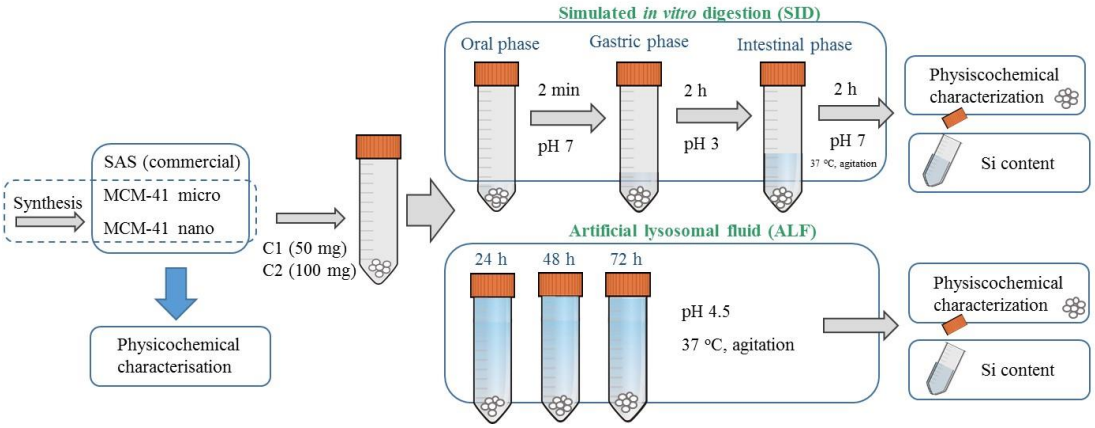

Fig. 2. Schematic representation of the experimental procedure.

2.5. Characterisation of silica particles

Materials were characterised before and at the end of the degradation tests (SID and 72 h of ALF) by three different techniques: transmission electron microscopy (TEM); zeta potential; dynamic light scattering (DLS). The TEM images were acquired by a Philips CM 10 microscope (Koninklijke Philips Electronics N.V., Eindhoven, the Netherlands) operating at an acceleration voltage of 80 kV. The zeta potential (ζ-potential) of the particles was measured by a Zetasizer Nano ZS (Malvern Instruments Ltd., Worcestershire, UK). Smoluchowsky's mathematical model was used to convert the electrophoretic mobility measurements into ζ-potential values. Particle size distribution was studied by DLS using a laser diffractometer (Mastersizer 2000, Malvern Instruments Ltd., Worcestershire, UK). The Mie theory was applied by considering a refractive index of 1.45 for all the particles, and absorption indices of 0.01 and 0.1 for the SAS particles and the MCM-41 particles, respectively. For the zeta potential and particle size distribution measurements, samples were diluted in distilled water and sonicated in an ultrasonic bath for 2 min to prevent the agglomeration of particles. All the determinations were made in triplicate.

2.6. Quantification of the silicon content in biological fluids

Supernatants were analysed to determine the total concentration of free silicon in each sample. In the SID study, due to the organic matter content of samples, aliquots were previously subjected to an acid digestion process in a microwave oven at 180ºC. Then the SID- and ALF-treated samples were all filtered and analysed by Inductively Coupled Plasma Mass Spectrometry (ICP-MS). An Agilent 7900 ICP-MS (Agilent Technologies LTd., CA, US) was used, equipped with a MicroMist nebulizer and a Scott spray chamber. The operating parameters were as follows; 1550 W of RF power, Ar gas flow rate 15 L/min, carrier gas flow rate 1.07 L/min. He and H_2 were employed as octopolar collision and reaction gases,

respectively. The percentage of dissolved Si was calculated by determining the dissolved Si from the original silica mass. The results were corrected by subtracting the analytical signal of the blanks from each sample.

2.7. Statistical analyses

The effect of treatment, particle type, concentration and functionalisation on zeta potential, particle size distribution and Si content were determined by a multifactor analysis of variance (ANOVA). A statistical analysis was carried out using Statgraphics Centurion XVI (Statpoint Technologies, Inc., Warrenton, VA, USA). The LSD (least significant difference) procedure was used to test the differences between averages at the 5% significance level.

3. Results and Discussion

3.1. Content of EOCs on the particles' surface

The TGA and elemental analyses of the functionalised particles showed that the yield of the immobilisation process was higher for the MCM-41 micro (values within the 1.5%-15% range), followed by MCM-41 nano (from 0.7% to 11%) and SAS (0.06% and 3%) for all the tested EOCs. The compound with the biggest anchorage yield was vanillin, followed by eugenol and carvacrol. The quantity of immobilised compound for each particle type was taken into account while calculating the fraction of Si dissolved in the degradation tests. For the SAS functionalised with carvacrol, the amount of immobilised compound was very small (0.06%). Therefore, this material type was not used for the subsequent analysis.

3.2. Characterisation of the bare and functionalised silica particles

The physico-chemical characteristics of the materials (e.g. morphology, particle size, surface charge) are major factors that affect their behaviour in biological systems and toxicity and should, therefore, be considered in their risk assessment.

Figure 3 shows the TEM images of the different bare and vanillin functionalised silica particles before SID and ALF exposure. The vanillin-functionalised particles were selected as an example because no differences were found between the different EOCs functionalised materials. The TEM images allowed us to observe the particle size, shape, porosity and internal structure of the materials. Information about the size and shape of the different silica particles is summarised in Table S1. Regarding the microstructure of the materials before both treatment types, SAS exhibited a globular sponge-like microstructure with smooth edges, MCM-41 micro were irregularly elongated and MCM-41 nano were uniformly spherical particles with a marked tendency to agglomerate. The TEM images of the MCM-41 particles also allowed us to observe

the characteristic hexagonal structure of mesoporous materials as alternate black and white lines (Fig. 3). Moreover, when comparing particles before and after functionalisation, we observed that this process neither altered the morphology or size of all three types of silica particles, nor affected the pore channel structure or porosity of the MCM-41 mesoporous materials, which confirms that their structure was preserved after the functionalisation process.

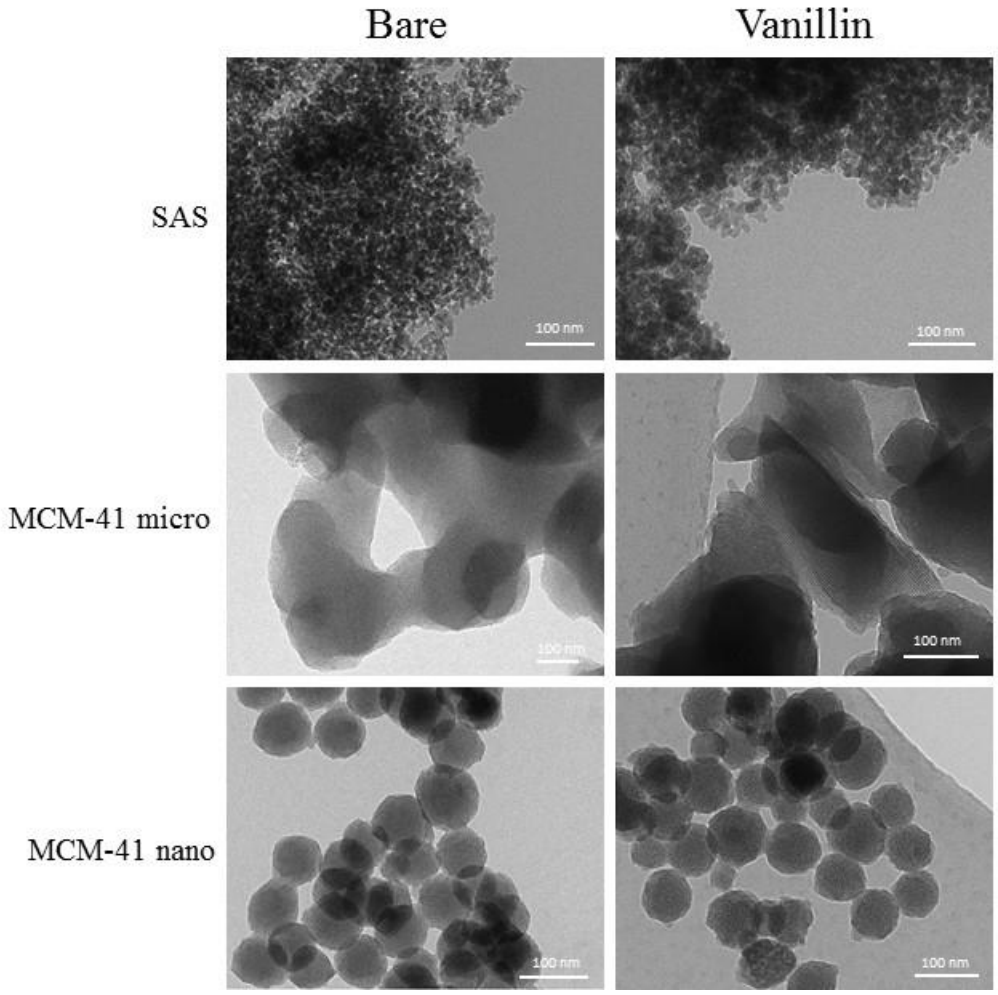

Fig. 3. Representative TEM images of the bare and vanillin functionalised SAS, MCM-41 micro and MCM-41 nano before SID and ALF exposures.

After SID or the 72-hour treatment with ALF, no changes in morphology, size or state of aggregation were observed for the bare or functionalised SAS and MCM-41 micro (Fig. 4). The TEM images revealed that the mesoporous structure of MCM-41 micro was preserved and no differences were found in the hexagonal network of the untreated and treated samples with both treatment types. However for the bare MCM-41 nano, contact with the digestion fluids led to loss of textural properties. As seen in Figure 4, after the SID procedure, the MCM-41 nano

surface was partially degraded and became irregular shaped, although their ordered mesoporous conformation remained. Unlike the bare nanoparticles, the functionalised MCM-41 nano presented the same morphology, particle size and porous structure both before and after treating this material with digestion fluids. Thus the immobilisation of the different EOCs on the surface of particles allowed their structure to be preserved during the SID process. Pérez-Esteve et al. (2016a) found that bare MCM-41 nanoparticles exhibited an evident degradation of their ordered structure, characterised by loss of specific surface area and pore volume as a result of the low pH of the gastric phase in the digestion process, while their microparticulated counterparts remained stable against degradation. These authors also found that the functionalisation of the silica MCM-41 nanoparticles with amines improved particle stability in the *in vitro* digestion procedure. The preservation of the mesoporous silica particles structure after organic functionalisation has also been observed by Izquierdo-Barba et al. (2010), who studied the long-term stability of bare and functionalised SBA-15 silica particles in different artificial physiological solutions. These authors reported the partial loss of the mesoporous structure of the unmodified particles, but the preserved structural properties of the SBA-15 particles functionalised with alkyl chains or aminopropyl groups.

The zeta potential values and particle size distribution of the bare and EOCs-functionalised particles before and after exposure to SID and 72 h of ALF are shown in Table 1. The effect of the different experimental factors (treatment, particle type, concentration and functionalisation) on both parameters was evaluated. The concentration of particles was not taken as a factor for the statistical analysis as it was previously verified that there are no significant differences ($p > 0.5$) between concentration levels.

The zeta potential results were significantly affected by all the studied factors and their interactions, and functionalisation was the most important factor (F-ratio = 12595.95). The most marked differences were found between the bare and functionalised particles, independently of the compound anchored to the surface of particles. The bared particles exhibited negative zeta potential values because silanol groups were present on their surface, while the functionalised materials obtained positive values because of the grafting of the EOC-alkoxysilane derivatives. This change in the zeta potential values confirmed the efficiency of the functionalisation process. Moreover, the zeta potential values did not change after the treatment with biological fluids, which confirmed that anchored compounds were preserved. When the zeta potential value fell outside the instability range (± 30 mV), particles remained dispersed and suspended. When the zeta potential fell within this range, particles tended to agglomerate. So, all the analysed particles fell within or around this range, and tended to form agglomerates.

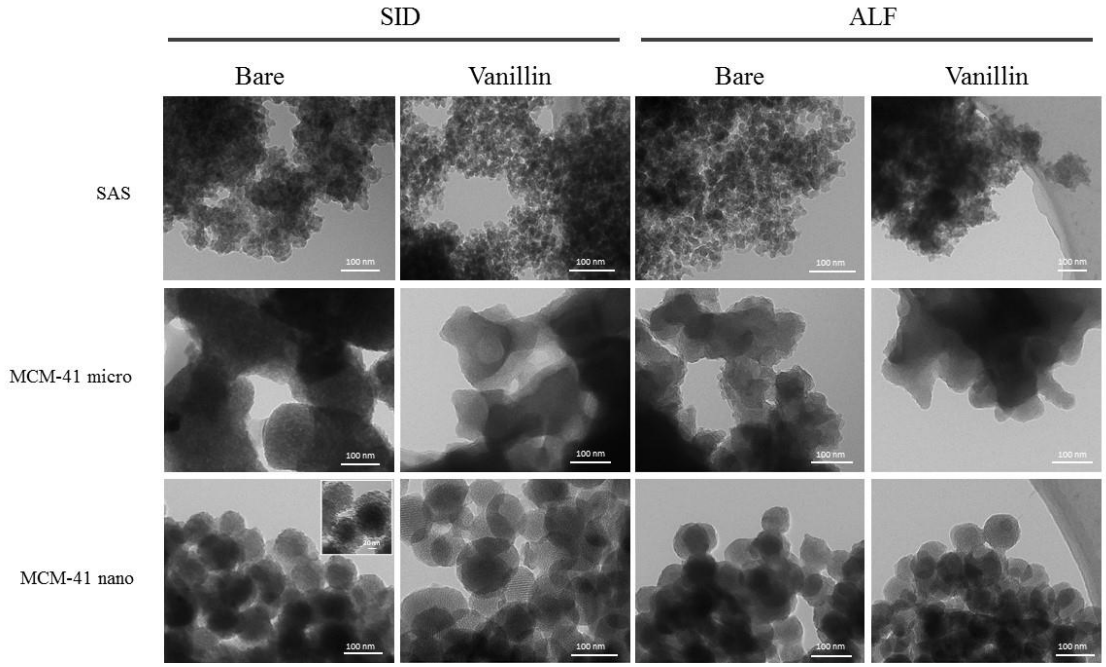

Fig. 4. Representative TEM images of the bare and vanillin functionalised SAS, MCM-41 micro and MCM-41 nano after SID and ALF exposure for 72 h.

Treating samples with ALF lowered the zeta potential values of particles, while the behaviour of the materials subjected to the SID process was similar to that of the untreated samples. Different properties of suspension media, such as pH, hardly influence the zeta potential values (Berg et al., 2009). In our study, the acidic nature of ALF facilitated the adsorption of ions of a complementary charge to the surface of particles by reducing the overall charge of materials, while the neutral pH of the intestinal phase of SID gave no significant differences to the untreated samples.

For particle size distribution, the most important factors were particle type, functionalisation, and the interaction between both. The particle size distribution analysis showed that the mean size of the bare SAS and MCM-41 micro was 3.34 (0.03) and 0.66 (0.01) μm, respectively. With MCM-41 nano, even though the individual mean diameter value found by TEM (64 (12) nm), the particle size distribution determined by DLS confirmed the strong tendency of this type of particles to agglomerate, and the secondary size diameter of the bulk material was 4.92 (0.06) μm. This trend to form large agglomerates found in MCM-41 nano could be explained by the stronger van der Waals forces and more marked Brownian movement found for smaller materials, which enhance interactions among particles (Oliveira and Andrada, 2019).

Regarding the effect of functionalisation on particle size distribution, the bare particles generally showed higher $d_{0.5}$ values than the functionalised materials. This effect was especially stronger for MCM-41 nano, for which particle size distribution lowered from 4.92 (0.06) to 0.70 (0.00) μm for the vanillin functionalised nanoparticles. This reduction in mean diameter size could be related to the steps included in the manufacturing of functionalised particles, such as milling or stirring, which could reduce the formation of agglomerates between adjacent particles.

Acidic conditions, the ionic strength of the solution or the presence of biopolymers have been demonstrated to promote particle agglomeration (McClements et al., 2017). However, in this study, exposure to SID and ALF did not modify the particle size distribution of the bare or functionalised materials. The results obtained for both treatment types were similar to those of the untreated samples, and revealed that the conditions used in these artificial media did not alter the primary size or state of aggregation of the analysed silica particles. Fashina et al. (2013) studied the dissolution of silica nanoparticles grafted with phthalocyanines on ALF. They observed that the aggregation level did not significantly change over a 96-hour period. Similarly, Sakai-Kato et al. (2014) found that silica hydrodynamic size was not affected by dispersion in fasted- and fed-state simulated gastric and fed-state simulated intestinal fluids. Consequently, other factors related to the properties of silica materials could also be responsible for the agglomeration state of particles under physiological conditions.

Table 1. The zeta potential and particle size distribution ($d_{0.5}$) values of the different bare and EOCs-immobilised silica particles before treatment (n.t.) and after dissolution in SID and ALF. Values are expressed as mean (SD).

		Zeta potential (mV)					**$d_{0.5}$ (μm)**				
			SID		**ALF**			**SID**		**ALF**	
Material	**Functionalisation**	**n.t.**	**C1**	**C2**	**C1**	**C2**	**n.t.**	**C1**	**C2**	**C1**	**C2**
SAS	Bare	-26.27 (2.31)	-28.08 (0.71)	-26.26 (0.68)	-18.31 (1.82)	-17.57 (1.22)	3.34 (0.03)	3.59 (0.19)	3.84 (0.18)	3.20 (0.12)	3.07 (0.03)
	Eugenol	8.95 (0.28)	2.70 (0.27)	2.23 (0.74)	5.38 (1.52)	5.03 (1.29)	4.05 (0.05)	3.68 (0.00)	3.95 (0.15)	4.06 (0.08)	4.10 (0.01)
	Vanillin	18.68 (1.44)	21.21 (0.79)	19.09 (1.63)	8.03 (0.99)	7.34 (0.64)	3.23 (0.03)	3.49 (0.03)	3.26 (0.31)	3.43 (0.04)	3.52 (0.07)
MCM-41 micro	Bare	-47.52 (1.79)	-33.63 (2.18)	-33.89 (2.18)	-22.96 (4.64)	-23.72 (1.55)	0.66 (0.01)	0.62 (0.02)	0.64 (0.00)	0.62 (0.01)	0.65 (0.03)
	Carvacrol	36.88 (1.08)	39.39 (4.73)	36.39 (2.55)	10.85 (0.62)	14.22 (0.75)	0.59 (0.00)	0.59 (0.01)	0.59 (0.00)	0.58 (0.00)	0.56 (0.01)
	Eugenol	5.34 (0.36)	4.61 (0.35)	-3.86 (1.93)	2.15 (1.06)	2.22 (0.19)	0.67 (0.01)	0.64 (0.01)	0.65 (0.01)	0.68 (0.06)	0.66 (0.00)
	Vanillin	39.83 (1.15)	41.27 (1.31)	38.37 (1.30)	17.34 (0.63)	17.14 (0.30)	0.59 (0.00)	0.61 (0.00)	0.61 (0.02)	0.62 (0.01)	0.63 (0.00)
MCM-41 nano	Bare	-37.60 (1.35)	-30.83 (1.91)	-33.08 (1.01)	-29.82 (4.94)	-28.71 (7.31)	4.92 (0.06)	4.82 (0.02)	4.80 (0.21)	4.95 (0.22)	4.89 (0.03)
	Carvacrol	22.82 (1.53)	29.44 (0.80)	30.73 (4.74)	12.79 (0.43)	12.80 (1.59)	3.37 (0.01)	3.03 (0.10)	3.04 (0.04)	3.25 (0.18)	3.33 (0.18)
	Eugenol	6.90 (0.78)	4.83 (1.14)	12.93 (3.32)	7.29 (2.25)	8.09 (3.23)	3.25 (0.07)	3.18 (0.01)	3.19 (0.10)	3.26 (0.11)	3.08 (0.06)
	Vanillin	29.19 (0.67)	27.02 (0.53)	31.32 (3.10)	13.02 (0.71)	10.05 (0.44)	0.70 (0.00)	0.68 (0.02)	0.69 (0.01)	0.70 (0.00)	0.70 (0.00)

3.3. In vitro degradation of the bare and functionalised silica particles

The degradation of the silica particles under the SID and ALF conditions was measured by quantifying the free dissolved Si in biological fluids. Figure 5 illustrates the percentage of dissolved Si (g dissolved Si per 100 g of initial silica) after SID, and also after 24, 48 and 72 h of ALF treatment.

The results obtained for both types of biological conditions were similar. Particle type was the most important factor to affect Si dissolution in SID (F-ratio = 267.75) and ALF (F-ratio = 1083, 85). Of the three types of silica particles herein analysed, MCM-41 micro showed the highest solubility, and reached a maximum percentage of 7.22 (0.5) under the SID conditions and 16.02 (1.89) after 48 h of the ALF treatment. In contrast, the lowest solubility levels went to SAS, with the Si content in dissolution falling within the 0.06-1.86% range for SID and within the 0.56-2.29% range for ALF. The lower solubility found for the SAS particles agrees with He et al. (2010), who observed lower degradation percentages and a milder degradation process for amorphous sol-gel derived silica than for MCM-41 particles in simulated biological fluids (pH 7.4, 37ºC). The mild degradation behaviour found for SAS particles was attributed to their non-mesoporous structure and smaller specific surface area. Different authors have pointed out that the most important variable to determine Si dissolution under experimental conditions is a larger surface area, which is usually related to a smaller particle size (Larson, 2010; Roelofs and Vogelsberger, 2004; Utembe et al., 2015). In this study, MCM-41 micro presented the narrowest hydrodynamic particle size distribution from all the studied materials and the highest solubility levels. Unlike what could be expected, loss of textural properties observed by TEM for the bare MCM-41 nano after SID (Fig. 4) did not correlate with a higher Si dissolved content. As previously mentioned, MCM-41 nano showed a high agglomeration tendency by reducing the surface of the mineral available to interact with the surrounding media, and explained the lesser degradation behaviour of these MCM-41 particles. Therefore, the surface erosion of this material type could be related not only to an increase in Si dissolution, but also to a reduction in the mechanical stability of particles and transformation into a new disorder phase (Pérez-Esteve et al., 2016a).

Functionalisation significantly reduced the amount of dissolved Si after exposure to both treatments, independently of the EOC anchored to the surface of particles. The carvacrol immobilised particles showed a lower Si dissolution level, while the eugenol functionalised particles were the least stable of all the functionalised materials. This increase in the stability of silica particles has also been observed after functionalisation with other organic groups. Lin et al. (2011) compared the stability of bare and pegylated mesoporous silica nanoparticles in two different biological media (PBS and DMEM). Their results showed that the amount of free Si

was significantly lower for the modified nanoparticles. Interestingly, the pegylation of particles improved their biocompatibility and decreased macrophage uptake, which renders them more suitable for human applications. Izquierdo-Barba et al. (2010) studied the long-term stability of SBA-15 silica particles in three different solutions that mimicked physiological fluids (a saline solution, an acellular aqueous solution similar to human plasma and DMEM) at 37ºC. These authors found that the largest amount of lixiviated Si went to bare SBA-15, regardless of the tested media. In contrast, the functionalisation of SBA-15 particles with alkyl chains (methyl and octyl) and aminopropyl groups lowered the degradation rate compared to the unmodified SBA-15 and helped to preserve their structural properties. This reduction in the amount of Si dissolved in the media of the modified samples was attributed to the formation of an organic coverage, which would act as a protection barrier. Other authors have suggested that some molecules, such as amine groups, attached to the surface of particles would also be able to locally neutralise the acidic environment created by SGF (Pérez-Esteve et al., 2016a).

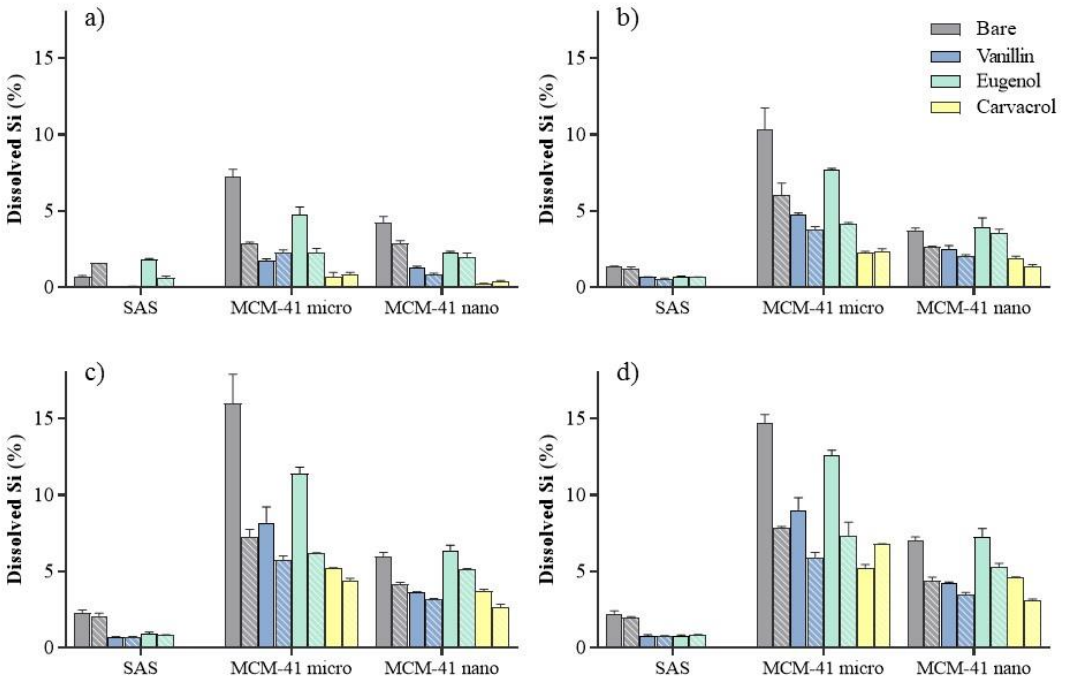

Fig 5. Percentage of dissolved Si after SID (a) and 24 (b), 48 (c) and 72 h (d) of ALF exposure. The plotted data represent the experimental results of three different particle types (SAS, MCM-41 micro, MCM-41 nano) at the C1 (straight bars) and C2 (dashed bars) particle concentrations.

A lower initial concentration of particles led to a higher bulk degradation percentage. Other studies have also observed that an increased silica concentration reduces the overall amount of

dissolved Si. Larson et al. (2010) found that a dissolved fraction of the 100 mg silica condition was 1.6-fold bigger that the dissolved fraction of 200 mg silica. He et al. (2010) also observed this phenomenon while studying the degradation behaviour of different MCM-41 types of mesoporous silica in simulated body fluid (SBF). In this media, a slow diffusion stage, caused by the deposition of a monolayer of calcium and magnesium species, was responsible for inhibiting silica dissolution. An increase in the initial silica concentration prolonged this degradation stage given the much bigger total surface area. Therefore, a much longer time was needed to cover the entire surface with calcium/magnesium silicates.

The solubility of silica particles depends on the pH of the dispersion medium and significantly increases under alkaline conditions. Larson et al. (2010) measured the dissolution rates of crystalline silica microparticles in a simulated lung fluid solution at different pHs over a 28-day period. These authors found that the samples in solution at pH 7.5 exhibited dissolution rates that were 2.0-3.5-fold higher than those achieved at pH 6.5 and pH 6.0, respectively. Braun et al. (2016) studied the dissolution kinetics of mesoporous silica particles in different physiological media to find that the dissolution rate of materials was lower in SGF (pH 1.6) than in other simulated biological buffers (pH 7.25-7.40). These differences were explained by the increasing deprotonation of silanol groups and the hydrolysis of the Si–O–Si-bonds catalysed by OH-nucleophiles, which occurred under alkaline conditions. Accordingly, an increased dissolution of the different silica particles in the intestinal phase of the *in vitro* digestion procedure could be expected. However in this study, all the materials presented higher levels of dissolved Si after the ALF exposure than under SID conditions, except for the eugenol immobilised SAS. In addition to pH, another important factor for determining the solubility of silica particles is the dispersion medium's composition. Together with alkali ions, the presence of Mg^{2+}, Ca^{2+} and Na^{+} ions, along with the presence of organic acid salts, enhance the dissolution rate of silica materials (Larson, 2010). So ALF contains a higher concentration of Na^{+} and Mg^{2+} ions than SID fluids, and includes citric acid and different salts of organic acids like sodium citrate, lactate or pyruvate, among others. At the same time, significant differences in the degradation kinetics of silica materials have been found depending on whether proteins are present or absent in the dissolution medium (Izquierdo-Barba et al., 2010). Protein adsorption on the surface of particles may prevent Si leaching from the particles by reducing the dissolution of particles under SID conditions.

If we take into account the exposure time of the particles in ALF, the analysis of the Si concentration in solution at the different time points revealed no significant differences between 48 and 72 h of exposure for the different materials. These results contrast with those reported by Fashina et al. (2013), who found that the solubility of silica nanoparticles in ALF still increased after 96 h exposure. However, lack of resemblance in the nature, size and agglomeration state of

the bulk materials could be responsible for these differences. The increased Si dissolution observed between 24 and 48 h of ALF exposure, and the short duration of SID compared to ALF, could indicate that not only the chemical composition of dissolution media, but also exposure time, could be important factors for determining differences in particle dissolution between both treatment types.

4. Conclusions

Due to the potential applications in the food industry of the silica particles that are our study object, it is necessary to provide information about the fate of these materials under conditions that represent oral exposure in order to predict possible toxicological responses. Agglomeration state and dissolution behaviour are key properties for determining the toxic responses of particles. A poor agglomeration state of particles induces their bioaccumulation, while high dissolution behaviour induces the enhanced release of ions to medium. Both conditions are related to increased inflammatory responses. The results found in this study show that the agglomeration state of the different particle types did not change under physiological conditions, and that no nanosized particles formed. Nanoparticles may more easily cross the intestinal barrier after oral ingestion and reach cellular compartments and, therefore, more toxic effects can be expected. In contrast, microparticles are more likely to be eliminated while reducing the risk of these materials accumulating after oral ingestion. All the studied materials displayed low dissolution behaviour under both simulated conditions. However, SAS was the most stable material, followed by MCM-41 nano and finally by MCM-41 micro. These findings suggest that agglomeration state and surface area are the two main factors that determine the degradation behaviour of silica particles. Moreover, functionalisation of silica particles with EOCs gave lower dissolution levels and, therefore, increased stability under both biological conditions. This effect could be attributed to the fact that EOCs derivatives immobilised on the surface of particles could act as a protection barrier by forming an organic coverage. Our results are relevant to understand the behaviour of these innovative silica particles under biological conditions and could help design new hybrid materials for oral applications. However, further research is necessary to study the stability behaviour of particles by taking into account the interactions of materials with components present in the food matrix or of the tissues that form the gastrointestinal tract. Safe applications of emerging materials should be guaranteed to minimise their impact on human health and the environment.

Acknowledgements

The authors gratefully acknowledge the financial support from the Spanish government (Project RTI2018-101599-B-C21 (MCUI/AEI/FEDER, EU)). Cristina Fuentes also thanks the *Generalitat Valenciana* for being funded by the predoctoral programme Vali+d (ACIF/2016/139). María Ruiz-Rico acknowledges the Generalitat Valenciana for her Postdoctoral Fellowship (APOSTD/2019/118).

References

ALOthman, Z., 2012. A Review: Fundamental Aspects of Silicate Mesoporous Materials. Materials. 5, 2874–2902. https://doi.org/10.3390/ma5122874

Berg, J.M., Romoser, A., Banerjee, N., Zebda, R., Sayes, C.M., 2009. The relationship between pH and zeta potential of ~ 30 nm metal oxide nanoparticle suspensions relevant to in vitro toxicological evaluations. Nanotoxicology 3, 276–283. https://doi.org/10.3109/17435390903276941

Braun, K., Pochert, Alexander, Beck, M., Fiedler, Richard, Gruber, J., Lindén, M., 2016. Dissolution kinetics of mesoporous silica nanoparticles in different simulated body fluids. J. Sol-Gel Sci. Technol. 79, 319–327. https://doi.org/10.1007/s10971-016-4053-9

Brodkorb, A., Egger, L., Alminger, M., Alvito, P., Assunção, R., Ballance, S., Bohn, T., Bourlieu-Lacanal, C., Boutrou, R., Carrière, F., Clemente, A., Corredig, M., Dupont, D., Dufour, C., Edwards, C., Golding, M., Karakaya, S., Kirkhus, B., Le Feunteun, S., Lesmes, U., Macierzanka, A., Mackie, A.R., Martins, C., Marze, S., McClements, D.J., Ménard, O., Minekus, M., Portmann, R., Santos, C.N., Souchon, I., Singh, R.P., Vegarud, G.E., Wickham, M.S.J., Weitschies, W., Recio, I., 2019. INFOGEST static in vitro simulation of gastrointestinal food digestion. Nat. Protoc. 14, 991–1014. https://doi.org/10.1038/s41596-018-0119-1

Cho, W.-S., Duffin, R., Thielbeer, F., Bradley, M., Megson, I.L., MacNee, W., Poland, C.A., Tran, C.L., Donaldson, K., 2012. Zeta Potential and Solubility to Toxic Ions as Mechanisms of Lung Inflammation Caused by Metal/Metal Oxide Nanoparticles. Toxicol. Sci. 126, 469–477. https://doi.org/10.1093/toxsci/kfs006

Colas, A., Rafidison, P., 2005. Silicones in new pharmaceutical developments from formulations to manufacturing processes. Pharma. Chem. 4, 46–49.

Croissant, J.G., Fatieiev, Y., Almalik, A., Khashab, N.M., 2018. Mesoporous Silica and Organosilica Nanoparticles: Physical Chemistry, Biosafety, Delivery Strategies, and

Biomedical Applications. Adv. Healthc. Mater. https://doi.org/10.1002/adhm.201700831

Diab, R., Canilho, N., Pavel, I.A., Haffner, F.B., Girardon, M., Pasc, A., 2017. Silica-based systems for oral delivery of drugs, macromolecules and cells. Adv. Colloid Interface Sci. 249, 346–362. https://doi.org/10.1016/j.cis.2017.04.005

Fashina, A., Antunes, E., Nyokong, T., 2013. Silica nanoparticles grafted with phthalocyanines: Photophysical properties and studies in artificial lysosomal fluid. New J. Chem. 37, 2800–2809. https://doi.org/10.1039/c3nj00439b

Flynn, J., Mallen, S., Durack, E., O'Connor, P.M., Hudson, S.P., 2019. Mesoporous matrices for the delivery of the broad spectrum bacteriocin, nisin A. J. Colloid Interface Sci. 537, 396–406. https://doi.org/10.1016/j.jcis.2018.11.037

García-Ríos, E., Ruiz-Rico, M., Guillamón, J.M., Pérez-Esteve, É., Barat, J.M., 2018. Improved antimicrobial activity of immobilised essential oil components against representative spoilage wine microorganisms. Food Control 94, 177–186. https://doi.org/10.1016/j.foodcont.2018.07.005

Hardy, A., Benford, D., Halldorsson, T., Jeger, M.J., Knutsen, H.K., More, S., Naegeli, H., Noteborn, H., Ockleford, C., Ricci, A., Rychen, G., Schlatter, J.R., Silano, V., Solecki, R., Turck, D., Younes, M., Chaudhry, Q., Cubadda, F., Gott, D., Oomen, A., Weigel, S., Karamitrou, M., Schoonjans, R., Mortensen, A., 2018. Guidance on risk assessment of the application of nanoscience and nanotechnologies in the food and feed chain: Part 1, human and animal health. EFSA J. 16. https://doi.org/10.2903/j.efsa.2018.5327

He, Q., Shi, J., Zhu, M., Chen, Y., Chen, F., 2010. The three-stage in vitro degradation behavior of mesoporous silica in simulated body fluid. Microporous Mesoporous Mater. 131, 314–320. https://doi.org/10.1016/J.MICROMESO.2010.01.009

He, Q., Zhang, Z., Gao, F., Li, Y., Shi, J., 2011. In vivo Biodistribution and Urinary Excretion of Mesoporous Silica Nanoparticles: Effects of Particle Size and PEGylation. Small 7, 271–280. https://doi.org/10.1002/smll.201001459

Henderson, R.G., Verougstraete, V., Anderson, K., Arbildua, J.J., Brock, T.O., Brouwers, T., Cappellini, D., Delbeke, K., Herting, G., Hixon, G., Odnevall Wallinder, I., Rodriguez, P.H., Van Assche, F., Wilrich, P., Oller, A.R., 2014. Inter-laboratory validation of bioaccessibility testing for metals. Regul. Toxicol. Pharmacol. 70, 170–181. https://doi.org/10.1016/j.yrtph.2014.06.021

Izquierdo-Barba, I., Colilla, M., Manzano, M., Vallet-Regí, M., 2010. In vitro stability of SBA-15 under physiological conditions. Microporous Mesoporous Mater. 132, 442–452.

https://doi.org/10.1016/J.MICROMESO.2010.03.025

Larson, R., 2010. Assessing the Solubility of Silicon Dioxide Particles Using Simulated Lung Fluid. Open Toxicol. J. 4, 51–55. https://doi.org/10.2174/1874340401004010051

Lin, Y.-S., Abadeer, N., Haynes, C.L., 2011. Stability of small mesoporous silicananoparticles in biological media. Chem. Commun. 47, 532–534. https://doi.org/10.1039/C0CC02923H

Lührs, A.-K., Geurtsen, W., 2009. The Application of Silicon and Silicates in Dentistry: A Review, in: Biosilica in Evolution, Morphogenesis, and Nanobiotechnology (pp. 359–380). Springer, Berlin, Heidelberg. https://doi.org/10.1007/978-3-540-88552-8_16

Manzano, M., Aina, V., Areán, C.O., Balas, F., Cauda, V., Colilla, M., Delgado, M.R., Vallet-Regí, M., 2008. Studies on MCM-41 mesoporous silica for drug delivery: Effect of particle morphology and amine functionalization. Chem. Eng. J. 137, 30–37. https://doi.org/10.1016/J.CEJ.2007.07.078

McClements, D.J., Xiao, H., Demokritou, P., 2017. Physicochemical and colloidal aspects of food matrix effects on gastrointestinal fate of ingested inorganic nanoparticles. Adv. Colloid Interface Sci. 246, 165–180. https://doi.org/10.1016/J.CIS.2017.05.010

Minekus, M., Alminger, M., Alvito, P., Ballance, S., Bohn, T., Bourlieu, C., Carrière, F., Boutrou, R., Corredig, M., Dupont, D., Dufour, C., Egger, L., Golding, M., Karakaya, S., Kirkhus, B., Le Feunteun, S., Lesmes, U., Macierzanka, A., Mackie, A., Marze, S., McClements, D.J., Ménard, O., Recio, I., Santos, C.N., Singh, R.P., Vegarud, G.E., Wickham, M.S.J., Weitschies, W., Brodkorb, A., 2014. A standardised static *in vitro* digestion method suitable for food – an international consensus. Food Funct. 5, 1113–1124. https://doi.org/10.1039/C3FO60702J

Oliveira, D.M., Andrada, A.S., 2019. Synthesis of ordered mesoporous silica MCM-41 with controlled morphology for potential application in controlled drug delivery systems. Ceramica 65, 170–179. https://doi.org/10.1590/0366-69132019653742509

Pennington, J.A.T., 1991. Silicon in foods and diets. Food Addit. Contam. 8, 97–118. https://doi.org/10.1080/02652039109373959

Pérez-Esteve, É., Ruiz-Rico, M., de la Torre, C., Llorca, E., Sancenón, F., Marcos, M.D., Amorós, P., Guillem, C., Martínez-Máñez, R., Barat, J.M., 2016a. Stability of different mesoporous silica particles during an in vitro digestion. Microporous Mesoporous Mater. 230, 196–207. https://doi.org/10.1016/J.MICROMESO.2016.05.004

Pérez-Esteve, É., Ruiz-Rico, M., de la Torre, C., Villaescusa, L.A., Sancenón, F., Marcos, M.D., Amorós, P., Martínez-Máñez, R., Barat, J.M., 2016b. Encapsulation of folic acid in

different silica porous supports: A comparative study. Food Chem. 196, 66–75. https://doi.org/10.1016/J.FOODCHEM.2015.09.017

Ribes, S., Ruiz-Rico, M., Pérez-Esteve, É., Fuentes, A., Barat, J.M., 2019. Enhancing the antimicrobial activity of eugenol, carvacrol and vanillin immobilised on silica supports against Escherichia coli or Zygosaccharomyces rouxii in fruit juices by their binary combinations. LWT 113, 108326. https://doi.org/10.1016/j.lwt.2019.108326

Ribes, S., Ruiz-Rico, M., Pérez-Esteve, É., Fuentes, A., Talens, P., Martínez-Máñez, R., Barat, J.M., 2017. Eugenol and thymol immobilised on mesoporous silica-based material as an innovative antifungal system: Application in strawberry jam. Food Control 81, 181–188. https://doi.org/10.1016/J.FOODCONT.2017.06.006

Roelofs, F., Vogelsberger, W., 2004. Dissolution Kinetics of Synthetic Amorphous Silica in Biological-Like Media and Its Theoretical Description. J. Phys. Chem. B 108, 11308–11316. https://doi.org/10.1021/jp048767r

Ruiz-Rico, M., Pérez-Esteve, É., Bernardos, A., Sancenón, F., Martínez-Máñez, R., Marcos, M.D., Barat, J.M., 2017. Enhanced antimicrobial activity of essential oil components immobilized on silica particles. Food Chem. 233, 228–236. https://doi.org/10.1016/J.FOODCHEM.2017.04.118

Sakai-Kato, K., Hidaka, M., Un, K., Kawanishi, T., Okuda, H., 2014. Physicochemical properties and in vitro intestinal permeability properties and intestinal cell toxicity of silica particles, performed in simulated gastrointestinal fluids. Biochim. Biophys. Acta - Gen. Subj. 1840, 1171–1180. https://doi.org/10.1016/J.BBAGEN.2013.12.014

Stebounova, L. V., Guio, E., Grassian, V.H., 2011. Silver nanoparticles in simulated biological media: a study of aggregation, sedimentation, and dissolution. J. Nanoparticle Res. 13, 233–244. https://doi.org/10.1007/s11051-010-0022-3

Stopford, W., Turner, J., Cappellini, D., Brock, T., 2003. Bioaccessibility testing of cobalt compounds. J. Environ. Monit. 5, 675–680. https://doi.org/10.1039/b302257a

Utembe, W., Potgieter, K., Stefaniak, A.B., Gulumian, M., 2015. Dissolution and biodurability: Important parameters needed for risk assessment of nanomaterials. Part. Fibre Toxicol. 12, 11. https://doi.org/10.1186/s12989-015-0088-2

Villota, R., Hawkes, J.G., 1986. Food applications and the toxicological and nutritional implications of amorphous silicon dioxide. C R C Crit. Rev. Food Sci. Nutr. 23, 289–321. https://doi.org/10.1080/10408398609527428

Wang, G., Otuonye, A.N., Blair, E.A., Denton, K., Tao, Z., Asefa, T., 2009. Functionalized mesoporous materials for adsorption and release of different drug molecules: A comparative study. J. Solid State Chem. 182, 1649–1660. https://doi.org/10.1016/j.jssc.2009.03.034